Melt Spinning of Poly(vinylidene fluoride) Fibers and the Influence of Spinning Parameters on β-Phase Crystallinity

Anja Lund,[1,2] Bengt Hagström[3]

[1]*Swedish School of Textiles, University of Borås, SE-501 90 Borås, Sweden*
[2]*Department of Materials and Manufacturing Technology, Chalmers University of Technology, SE-412 96 Gothenburg, Sweden*
[3]*Textiles and Plastics Department, Swerea IVF, Box 104, SE-431 22 Mölndal, Sweden*

Received 27 August 2009; accepted 12 November 2009
DOI 10.1002/app.31789
Published online 27 January 2010 in Wiley InterScience (www.interscience.wiley.com).

ABSTRACT: The effects of melt-spinning and cold-drawing parameters on the formation of β-phase crystallinity in poly(vinylidene fluoride) (PVDF) fibers and ways of increasing such crystallinity were studied. Fibers were melt-spun with four different melt draw ratios (MDRs) and were subsequently cold-drawn at different draw ratios (λ). The maximum λ value in cold drawing was dependent on the MDR used in melt spinning. The crystalline structure of the fibers was studied mainly with differential scanning calorimetry (DSC) and X-ray diffraction (XRD). The results showed that the degree of crystallinity in the fibers was determined by the MDR and that before cold drawing the crystalline structure of the fibers was predominantly in the α form. By cold drawing, α-phase crystallites could be transformed into the β phase. It was established that, under certain conditions of melt spinning and cold drawing, PVDF fibers of up to 80% crystallinity, mainly in the β form, could be prepared. It was further proposed that fibers spun at a sufficiently high MDR consist to a large extent of extended-chain crystals, and this greatly affects the melting point of PVDF. Thus, DSC melting-point data were shown to be insufficient for determining the crystalline phase of PVDF.
 J Appl Polym Sci 116: 2685–2693, 2010

Key words: fibers; differential scanning calorimetry (DSC); WAXS

INTRODUCTION

Poly(vinylidene fluoride) (PVDF) is a polymorphic polymer that, when made to crystallize in its polar form, yields piezoelectric and pyroelectric properties. In recent years, PVDF has found its way toward intelligent textile applications. Researchers have attempted to create, for example, sensors for cardiorespiratory monitoring during sleep to be placed under bed sheets[1,2] or integrated into belts,[3] wearable sensors to be placed on fingertips for reading Braille,[4] and energy-harvesting devices inside shoes.[5] In all these examples, sensors were constructed by the addition of a commercially available PVDF film to a textile material. This article is the first step in investigating the possibilities of creating an electroactive fiber or yarn for true integration into textile materials.

Crystalline forms of PVDF

PVDF is known to exist in at least four crystal forms, which are designated α, β, γ, and δ. The crystalline structure and the formation of the piezoelectric β polymorph in particular have been well explored in the case of PVDF films.[6–9] Although the nonpolar α phase is usually formed during crystallization from the melt or in solution-cast films, the polar β phase can be created by mechanical deformation of α-phase material. The two polymorphs exhibit different chain conformations. The α-phase chains have a TGTG′ conformation (G = gauche; T = trans), and its crystals consist of a monoclinic unit cell. The structure is nonpolar because of the cancellation of the dipoles exhibited by the two polar chains that make up the cell. The β-phase unit cell is orthorhombic and consists of two chains in an almost planar all-trans conformation. This structure is polar and can thus be useful as a base for a piezoelectric material.[10,11] The conformation of the γ phase is TTTGTTTG′, and it appears in PVDF crystallized at a high temperature and/or under a high pressure. The γ phase readily transforms into the β phase when it is mechanically deformed.[12] The δ phase is a polar version of the α phase; the chain conformation and unit cell dimensions are similar to those of the α phase, but the two chains in the cell pack so that their dipoles reinforce one another. A δ-phase PVDF is produced by the subjection of a film of α-phase PVDF to an electric poling field.[12,13]

Correspondence to: A. Lund (anja.lund@hb.se).

As mentioned previously, the β phase can be formed by mechanical deformation of α-phase material, and several researchers have attempted to find the optimal drawing parameters for producing PVDF films with a high content of β-phase crystallites. It has been found that the formation of a necking region during drawing is advantageous, and the draw ratio (λ) as well as the draw rate should be as high as possible for maximum α-to-β transformation to take place.[7,8] The drawing temperature for maximum α-to-β transformation is in the range of 80–90°C. A drawing temperature exceeding 90°C gives a lower relative β-phase content.[6–8]

Fiber spinning of PVDF

There is an important difference between manufacturing melt-spun fibers and casting films from the melt or solution. During melt spinning, fibers are subjected to uniaxial drawing at high rates before and during crystallization, and this introduces a strong elongational flow creating a molecular orientation that in turn leads to an increase in both the crystallization temperature and the crystallization rate.[14,15] Crystallization under orientation also affects the morphology. Spherulites may be found only in fibers spun at very low take-up velocities. Already at small orientations, the spherulites flatten in the direction of the orientation, and the structure in an orientation-crystallized polymer is normally one in which the lamellae are oriented perpendicularly to the orientation axis and are nucleated on and epitaxially grown from a flow-induced precursor structure of highly oriented and extended polymer chains, or shishes. The result is a shish-kebab structure.[15] Under weak orientations, the extended chains, or shishes, are very far apart. As the spin-line stress is increased, the rate of nucleation of shishes is enhanced (more amorphous polymer is converted to shishes), and the spacing between the shishes decreases.[11]

A structural model describing the crystallization process in the melt spinning of PVDF has been developed from online small-angle X-ray scattering and wide-angle X-ray scattering studies.[16] Two crystallization steps have been suggested: in the first step, the shish structure is formed, and in the second step, volume-filling crystallization takes place, and the kebab regions form from radial overgrowth along the shishes. This description is supported by other authors[11] who have noted that, in the melt spinning of PVDF with take-up speeds in the range of 10.6–61.0 m/min, only α-phase crystallinity is present except at the highest speed used, at which a very weak reflection from the β010 crystal plane can be seen.

Other researchers have conducted offline studies of orientation development and crystallization in PVDF fibers[17] spun at melt draw ratios (MDRs) ranging from 20 to 747, and the results of differential scanning calorimetry (DSC) measurements have been interpreted as showing that fibers spun at a spin-line stress (which is related to the drawdown ratio and molecular weight) exceeding a certain minimum level have β-phase crystallinity of up to 50.8 vol %. It has been suggested that the β phase develops at a certain degree of orientation in the melt. In our work, we found that DSC data alone were not sufficient to explain the type of crystallinity. Furthermore, in our fibers, the β phase developed only after a cold-drawing step.

In fiber production, melt spinning is generally followed by cold drawing (drawing at a temperature below the crystal melting point) of the fiber, as undrawn fibers exhibit poor mechanical properties, such as low stiffness, high strain to break, and high irreversible extensibility. Drawing is an irreversible elongation of an as-spun material in the solid state. This elongation is accompanied by an extension and orientation of macromolecules and crystallites along the fiber axis, and the orientation increases with increasing λ.[15] In a study of the hard elasticity behavior of PVDF fibers,[18] it was found that the β phase was induced by cold drawing of the fibers, but the total crystallinity was not affected. The ratio of the β phase to the α phase was very dependent on the temperature of drawing, the optimal temperature being 70°C. Moreover, an increase in the deformation rate and/or λ led to an increase in the ratio of the β phase to the α phase. Fibers were drawn up to 80%, and the maximum proportion of the β phase that was achieved was 22%.

In an interesting article,[19] it was argued that the creation of defects during crystallite breakage may be important for the α-to-β crystal phase transformation to take place. PVDF fibers spun at various take-up speeds (10.6–61.0 m/min) were examined during cold drawing by *in situ* small-angle X-ray scattering and wide-angle X-ray scattering measurements. Fibers were drawn up to 140%. The results showed that the bulk crystallinity was constant throughout drawing, but the β-to-α ratio increased with increasing strain. It was suggested that as drawing continues, the crystalline phase begins to shear apart, and α crystallites begin to deform into small crystallites, some of which convert into the β form. The mechanism behind this would be substantial internal rotation of the chain that begins to take place at defective sites, at which the interchain interaction is relatively weak. This rotation facilitates the transformation of the chain conformation from the TGTG′ form to the all-trans form.

Aim of this study

In this study, we attempted to determine how spinning and drawing parameters should be adjusted to enable fibers to be produced with high β-phase crystallinity. X-ray diffraction (XRD) and DSC were used to evaluate the crystalline structure. To the best of our knowledge, there has been no previous study of the combined influence of melt-spinning and cold-drawing parameters on high-β-phase-content PVDF fibers.

EXPERIMENTAL

Materials

The polymer was a PVDF homopolymer in pellet form supplied by Solvay Soleris (Milan, Italy), under the commercial name Solef 1010. The number-average and weight-average molecular weights (as given by the supplier) were 153×10^3 and 352×10^3, respectively. The average melt flow index was 6 g/10 min under a load of 5 kg at 230°C.

Sample preparation

Melt spinning

PVDF was melt-spun into monofilament fibers from a CEAST (Pianezza TO, Italy) Rheoscope 1000 capillary rheometer with a capillary die with a diameter of 1 mm and a length/diameter ratio of 40. All fibers were spun at 240°C and at a piston speed (V_P) of 5 mm/min. They were spun through air at room temperature to a take-up wheel with various speeds (V_T). After spinning, the fibers were transferred from the take-up wheel to a small bobbin.

The melt velocity (V_M) was calculated as follows:

$$V_M = V_P(d_{\text{cyl}}/d_{\text{cap}})^2 \tag{1}$$

where d_{cyl} is the diameter of the cylinder holding the polymer melt (9.5 mm) and d_{cap} is the diameter of the capillary. The MDR was calculated as follows:

$$\text{MDR} = V_T/V_M \tag{2}$$

The diameters of the fibers were measured with a micrometer. The values of the spinning velocities, MDRs, and final diameters of the melt-spun fibers are given in Table I.

TABLE I
Melt-Spinning Parameters and Diameters of the Fibers After Drawing in the Melt

Fiber	V_M (m/min)	V_T (m/min)	MDR	Average diameter (μm)
PVDF-MDR42	0.451	18.8	42	140 ± 5
PVDF-MDR84	0.451	37.7	84	98 ± 5
PVDF-MDR251	0.451	113.1	251	51 ± 2
PVDF-MDR419	0.451	188.4	419	35 ± 2

Cold drawing

From the bobbin, fibers were cold-drawn with two godets from Fourné Polymertechnik GmbH (Alfter, Germany). In all cold-drawing experiments, the temperature of the first godet was set to 80 ± 2°C, and that of the second godet was 23 ± 2°C. The speeds of the godets could be varied individually between 3 and 28 m/min. The godets were placed 395 mm apart. In cold drawing, λ is determined as follows:

$$\lambda = \frac{V_2}{V_1} = \frac{L}{L_0} \approx \frac{A_0}{A} \tag{3}$$

where V_1 and V_2 are the speeds of rotation of godets 1 and 2, respectively; L_0 and L are the specimen lengths before and after drawing, respectively; and A_0 and A are the cross-sectional areas before and after drawing, respectively. The nominal deformation rate ($\dot{\varepsilon}$) was calculated as follows:

$$\dot{\varepsilon} = \frac{V_2 - V_1}{x} \tag{4}$$

where x is the distance between the godets.

Characterization

Tensile testing

Tensile tests were carried out at room temperature in a Tinius Olsen H10KT tensile machine (Tinius Olsen Inc., Horsham, Philidelphia, PA) with single bollard grips suitable for fibers. The data were analyzed with Tinius Olsen software (QMat 5.41a). The drawing speed was 1000 mm/min, the gauge length was 100 mm, and the elongation of the specimen was calculated from the crosshead displacement. The results are based on measurements of five specimens from each fiber.

DSC

DSC analyses were carried out with a TA Instruments (New Castle, DE) DSC Q1000. Specimens were prepared with tweezers to roll small amounts of the continuous fiber into a ball. The ball was placed in an aluminum sample holder that was crimp-closed. All samples weighed 8.5 ± 0.5 mg. DSC scans were carried out at 60–220°C at a heating rate of 10°C/min. The results that are shown are from the first heating. They were analyzed with TA Instruments software (Universal Analysis 2000). The crystalline fraction (X_c) was calculated as follows:

$$X_c = \frac{\Delta H_m}{\Delta H_m^0} \times 100\% \quad (5)$$

where ΔH_m is the experimental heat of fusion and ΔH_m^0 is the heat of fusion of the 100% crystalline polymer. The value of ΔH_m^0 for PVDF was taken to be 104.7 J/g,[20] and ΔH_m was calculated from the area of the endothermic melting peak(s). DSC measurements were made of several samples of fibers spun on at least four different occasions for each set of spinning parameters. Although there was some variation in the sizes of the peaks, the trends remained unchanged and were clear. There was good repeatability in the positions of the peaks; the thermograms displayed in this article show representative results.

XRD

X-ray diffractograms were obtained with a Bruker AXS Inc. (Madison, WI) D8 Advance Theta X-ray diffractometer with a monochromator. The radiation source was Cr Kα with a wavelength of 2.28970 Å. An increment step of 0.1° and a rate of 1 step per 10 s were used. During the measurements, the sample was rotating at 30 rpm. All measurements were made at room temperature. The samples consisted of parallel fibers mounted on a flat sample holder by means of double-sided adhesive tape, and the direction of the X-ray beam was normal to the fiber axis. Fibers were mounted so that they covered the whole surface of the sample holder. XRD measurements were made of several samples of fibers spun on at least four different occasions for each set of spinning parameters. The results showed that although there was some variation in the sizes of the peaks, the trends remained unchanged and were clear. There was good repeatability in the positions of the peaks; the diffractograms displayed in this article are representative for these measurements.

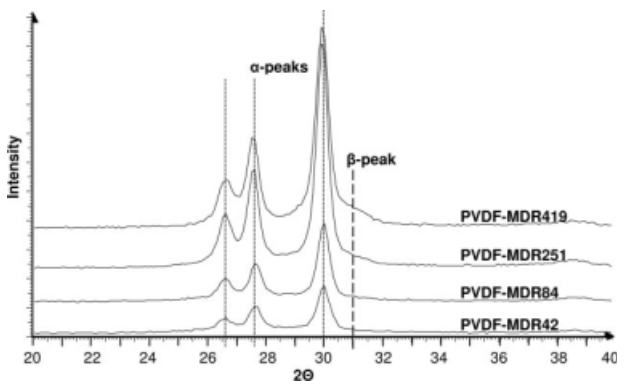

Figure 1 X-ray diffractograms of fibers drawn only in the melt.

TABLE II
Interplanar Distances and Corresponding 2θ Angles for the Maximum Intensity Peaks in XRD According to the Literature

α phase[10,17,21–24]			β phase[10,17,21–23,25,26]		
hkl	*d* (Å)	2θ (°)	*hkl*	*d* (Å)	2θ (°)
110	4.39–4.45	29.8–30.2	110/200	4.23–4.33	30.7–31.4
200	4.79–4.82	27.5–27.7			
010	4.92–5.10	26.0–26.9			

RESULTS AND DISCUSSION

Degree of crystallinity and β-phase content of the fibers drawn only in the melt

The results of the XRD characterization of melt-spun PVDF fibers are shown in Figure 1. Maximum intensity peaks, which correspond well to the reported distances between planes in α-phase crystallites, are present. The interplanar distances and corresponding 2θ angles are listed in Table II. On the XRD patterns for fibers spun with the two highest MDRs, there is a very small shoulder that may be interpreted as an indication of β-phase crystallites. Clearly, there is at the most very little β-phase crystallinity present in fibers drawn only in the melt.

Figure 2 shows DSC curves for the melt-spun fibers. All the fibers show an endothermic melting peak around 173°C. The fibers spun at MDRs of 251 and 419 also exhibit a melting peak at approximately 193°C. The areas of the melting peaks show that the degree of crystallinity is around 60% for fibers spun at the lower MDRs, but it increases dramatically to 80 and 90% at MDRs of 251 and 419, respectively, and this indicates the presence of orientation-induced crystallization.

It is interesting to note the second melting peak appearing at 193°C in the fibers spun at high MDRs. Other authors[17,20,27] have noticed a similar peak and

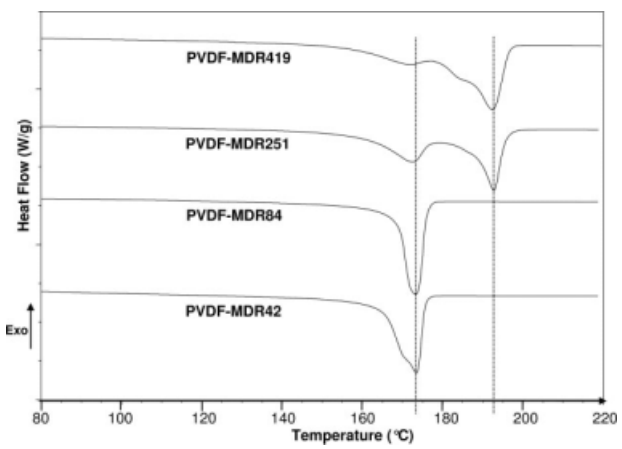

Figure 2 DSC thermograms of fibers drawn only in the melt.

TABLE III
Parameters of Cold Drawing

Fiber	λ	V_1 (m/min)	V_2 (m/min)	$\dot{\varepsilon}$ (min^{-1})
PVDF-MDR42	2	3	6	7.6
	4	3	12	22.8
	5	3	15	30.4
	6	3	18	38.0
PVDF-MDR84	2	3	6	7.6
	3	3	9	15.2
PVDF-MDR251	2	3	6	7.6
	2	6	12	15.2
PVDF-MDR419			Not cold-drawn	

have taken it as evidence of the existence of a β phase in PVDF. In our work, this conclusion is clearly contradicted by the XRD results, which show that there is hardly any β phase present in the fibers. Instead, we believe that the second higher melting peak may be associated with the formation of extended-chain crystals in the highly oriented melt at a high MDR, as will be further discussed.

Degree of crystallinity and β-phase content after cold drawing

Melt-spun fibers were cold-drawn according to Table III. The fibers were drawn up to the maximum λ value at which it was still possible to maintain a stable drawing process. It can be seen that these values correspond quite well to the values of the strain to break in Figure 3. PVDF-MDR419 (where the number following "MDR" is the melt draw ratio value) could not in practice be cold-drawn.

Figure 4 shows XRD patterns for the PVDF-MDR42 fibers before and after cold drawing. First at $\lambda = 2$, a shoulder appears at $2\theta \approx 31^\circ$, and this indicates the formation of β-phase crystallites. The three α peaks, which are dominant in the undrawn fiber, become broadened and of lower intensity, and this indicates the destruction of the original α-phase crystallites. As λ increases, the β peak grows, and the α peaks gradually disappear. At $\lambda = 5$ and $\lambda = 6$, there is almost complete conversion from α-phase crystallinity to β-phase crystallinity in the fibers.

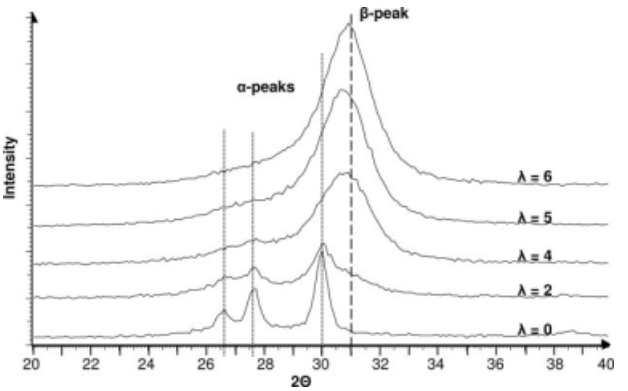

Figure 4 X-ray diffractograms of PVDF-MDR42 fibers before and after cold drawing.

Figure 5 shows a similar trend in the cold-drawn PVDF-MDR84 fibers: as λ increases, the β peak grows and the α peaks gradually disappear, although in these fibers, the maximum λ value was not sufficient for complete conversion from the α phase to the β phase. In PVDF-MDR251, drawing also led to the introduction of the β phase (see Fig. 6), but complete conversion was not achieved at the maximum λ value. These fibers were also drawn at a higher drawing rate with the same λ value, with the result that the content of β-phase crystallites increased at the expense of α-phase crystals. It seems that the drawing rate is an important factor for the conversion of the α phase to the β phase, and this may indicate that local heat dissipation and temperature play a role. It should be noted that in the PVDF-MDR42 and PVDF-MDR84 fibers, the increase in λ was accompanied by an increase in the draw rate, so the effects of these processes cannot be clearly separated.

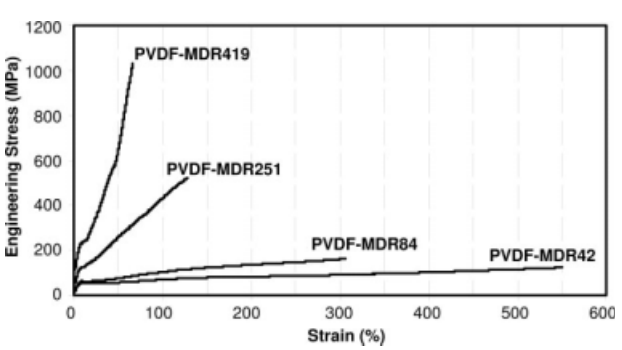

Figure 3 Engineering stress–strain curves for fibers drawn only in the melt.

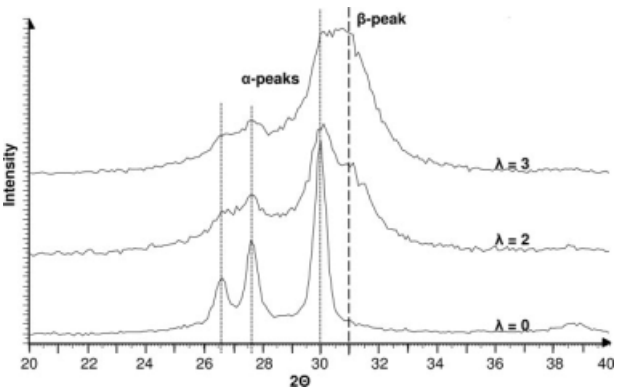

Figure 5 X-ray diffractograms of PVDF-MDR84 fibers before and after cold drawing.

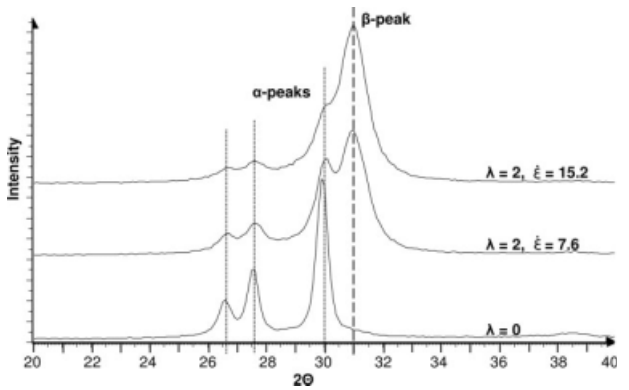

Figure 6 X-ray diffractograms of PVDF-MDR251 fibers before and after cold drawing.

Morphology of the fibers as interpreted from XRD and tensile test results

Interestingly, there is a distinct difference in the appearance of the β peaks in the cold-drawn PVDF-MDR251 and in the other two fibers. In the fibers spun at MDRs of 42 and 84, the β phase is indicated by a broad peak, which apparently includes some remains of the α peaks, which were in turn clearly broadening while disappearing. In contrast, the β-phase peak of PVDF-MDR251 is seen as a sharp individual peak of growing intensity, and the α peaks are reduced in intensity but not smeared out as in the other fibers. The broadening of peaks in XRD patterns may be due to small crystal sizes. Peak broadening may also be explained by defects in the crystalline lattice due to the occurrence of unit cells with deviating dimensions; this is a phenomenon not uncommon in polymer crystals.[28] In this work, interpreting the broad peak as a sign of small crystallites is in conformity with the hypothesis previously mentioned: phase transformation in PVDF occurs by the deformation of α crystallites into smaller crystallites, some of which then convert into the β form.[19] An alternative interpretation is that the broad peaks are indicative of a defective crystalline structure in which phase transformation first occurs at isolated sites within α crystallites. Thus, in the early stages of transformation, the crystalline structure is one in which β-phase crystallites are embedded in a matrix of the α phase, whereas after drawing up to $\lambda = 5$ or $\lambda = 6$, crystallites are predominantly β-phase with some α-phase defects.

The appearance of a singular β peak as in PVDF-MDR251 seems instead to indicate the formation of new crystallites purely in the β form. However, as the DSC results showed, the total degree of crystallinity in all the fibers remained unchanged. It may be speculated that, in the fiber spun at a higher MDR, there are more extended-chain crystals, and the chains in these parts begin to rotate and convert from the TGTG′ α conformation to the all-trans β conformation, which allows for the conversion of a whole crystallite rather than small portions of it.

To further investigate the crystalline structure of fibers drawn only in the melt, the behavior under a tensile load was studied. Figure 3 shows the engineering stress as a function of strain during drawing at room temperature. As can be seen in the graph, there is an essential difference in the tensile behavior between fibers spun at high MDRs and fibers spun at low MDRs, and this probably indicates a difference in the morphologies of the respective fibers. It is known from the literature[11,19,29,30] that molecular and crystalline orientation increases with increasing MDR, and we have shown that this is also true for the degree of crystallinity. This explains the increase in the initial modulus with increasing MDR, as available amorphous chains will be fewer when the degree of crystallinity increases, and these amorphous chains are already highly extended because of the increase in orientation. There will also be less possibility of lamellar tilting when the lamellae are already strongly oriented. However, it is thought[31] that after yielding, drawing proceeds by chain unfolding from the crystallites. The great resistance to drawing in samples PVDF-MDR251 and PVDF-MDR419 may imply that the chains involved in crystallites are already highly extended and thus cannot be unfolded.

Morphology of the fibers as interpreted from the DSC results

DSC results for selected fibers after cold drawing are shown in Figure 7. First, it may be noted that cold drawing does not cause any change in the degree of crystallinity of the fibers. Apparently, crystallinity is controlled only by the melt-spinning process. Figure 8 shows the degree of crystallinity as a function of MDR before and after cold drawing. Numbers are averages from three DSC measurements, and the

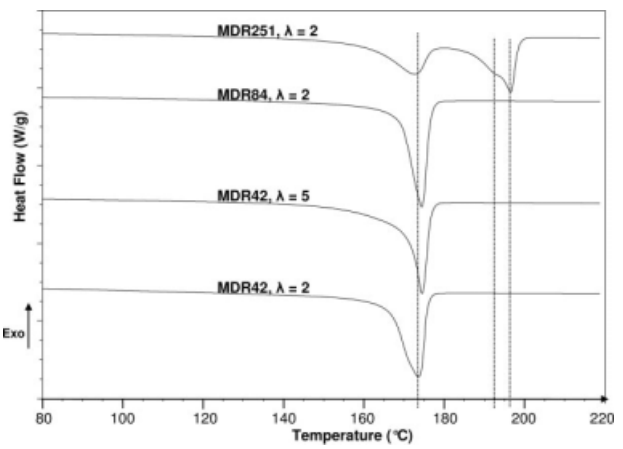

Figure 7 DSC thermograms of fibers after cold drawing.

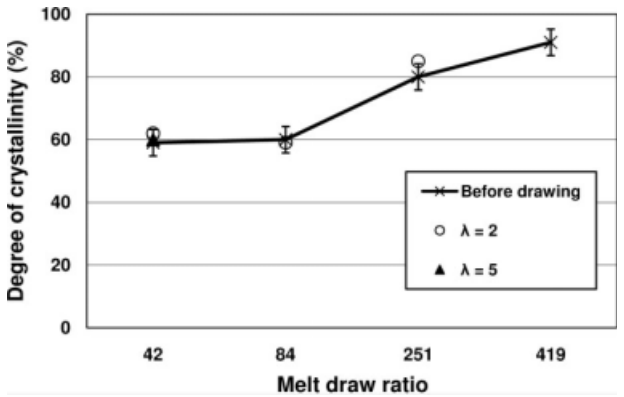

Figure 8 Degree of crystallinity with respect to MDR and the degree of cold drawing.

error bars represent the maximum standard deviation found in these measurements.

The shape of the DSC curves also provides valuable information about the fiber morphology. The two bottom curves (Fig. 7) represent PVDF-MDR42 at two different λ values. The fiber drawn at a higher λ value has a narrower melting peak, and the peak value is 1–2° higher than that of the fiber drawn at a lower λ value. The same observations can be made when the peak for PVDF-MDR84 drawn at $\lambda = 2$ is compared with that for the same fiber before drawing. It should be noted that no second melting peak appeared, even though β-phase crystallites were present in all these fibers. The fiber PVDF-MDR42, drawn at $\lambda = 5$, consisted almost exclusively of β-phase crystallites according to the XRD scans; still, there is no higher melting peak corresponding to β crystals present in the thermogram.

A broadened melting peak in DSC generally implies that there is a broad distribution of lamellar thicknesses in the crystallites, and so the thinning of a melting peak means that perfection of the crystallites has occurred during drawing. This may contradict the theory of lamellae breaking into smaller pieces during phase transformation. Instead, it could support the suggestion that α-to-β phase transformation occurs in one crystal body. The result of this is that the DSC data, not capable of distinguishing between α and β phases in one crystal body, simply show that crystals have become thicker and more uniform in size.

The thermogram for PVDF-MDR251 at $\lambda = 2$ (Fig. 7) has a completely different appearance: two peaks around 172 and 193°, which were present before drawing, are still seen in the same positions, but a new peak has appeared at 196°. The most common reasons for multiple endothermic melting peaks measured by DSC are reorganization and/or recrystallization of crystals during the slow heating in the calorimeter.[32] This may be particularly true for fibrous samples, as these are highly oriented and prone to changing their physical shape when heated. For example, several authors[32,33] have shown that the thermal behavior of polyethylene (PE) fibers depends largely on applied constraints; the fixation of the fibers in the DSC sample holder allowed a transition from the orthorhombic phase to the hexagonal phase in PE to take place in the course of the DSC experiments. Consequently, two new peaks appeared that were attributed to this transition and the subsequent melting of the new phase. Similar effects could have an impact in this case. However, in this work, all samples for DSC were prepared in the same way. Therefore, even though some phase transition may take place in DSC, it is different for the different fibers, and this indicates that there must be differences in the initial molecular structures.

Instead, we believe that the new melting peak appearing around 193°C in the fibers spun at high MDRs may be associated with the formation of extended-chain α-phase crystals. An increase in the melting temperature is consistent with an increase in the crystal thickness, as shown by the Thomson–Gibbs equation:[32]

$$T_m = T_m^0\left(1 - \frac{2\gamma_i}{\Delta H_m^0 l_c \rho_c}\right) \tag{6}$$

where T_m is the experimentally determined melting point, T_m^0 is the equilibrium melting point of the crystals, γ_i is the free surface energy of the lamellar fold surfaces, l_c is the thickness of the crystal, ρ_c is the density of the crystal, and ΔH_m^0 is the melting enthalpy of a fully crystalline polymer.

As previously mentioned, it has been shown[11] that, during the melt spinning of PVDF, the rate of nucleation of shishes increases with increasing spinline speed. This could support the idea that in our fibers spun at high MDRs, there is a large concentration of extended-chain crystals (forming the shish), whereas in the fibers spun at low MDRs, the occurrence of extended-chain crystals is too low to be picked up by DSC measurements. Other studies have shown that for PE, the melting temperature of a shish is about 15–20°C higher than that of PE spherulites or lamellae,[34] and for isotactic polypropylene, the melting temperature of a shish is 20–25°C higher than that of kebabs, which in turn have a melting temperature 5–10°C above that of unoriented crystals.[35] Thus, it seems not unlikely that the increase of 20°C in the melting temperature of our samples could be attributed to the melting of shish crystals. However, one must question whether such a high content of shish crystals in the fibers is realistic. If we assume that the heats of fusion of extended-chain crystals and of folded lamellar crystals are the same, the peak areas indicate that before

drawing, 45% of the crystallites in PVDF-MDR251 and 60% of the crystallites in PVDF-MDR419 consisted of extended-chain crystals. It may instead be suggested that the high melting point in our fibers comes not from shish crystals but rather from extended-chain crystals in the form of high-thickness lamellae.

An alternative explanation for the increase in the melting temperature could be that molecules in the amorphous structure become highly oriented in the course of high-speed spinning and subsequent drawing. When the degree of crystallinity is high, the relaxation of oriented amorphous chains will also be sterically restricted at high temperatures. This in turn may lead to a lower change in entropy (Δs) upon crystal melting, so the melting point would be higher according to the following thermodynamic relationship:

$$T_m = \frac{\Delta h}{\Delta s} \tag{7}$$

where Δh is the change in enthalpy. This hypothesis, however, raises the question of why there are two different melting temperatures rather than a higher melting temperature for the whole sample.

It must be concluded that the details of the morphology of our fibers are not fully understood. The questions raised here will be further pursued in a separate study.

Optimization of β-phase crystallinity

The results have shown that the degree of crystallinity can be significantly increased by an increase in the MDR during melt spinning, and before cold drawing, fibers consist predominantly of the α phase. The increase in crystallinity reduces the drawability. It has also been shown that increasing λ leads to a higher conversion from α-phase crystallinity to β-phase crystallinity. Thus, there is an antagonistic effect between the degree of crystallinity and the possibility of conversion from the α phase to the β phase. An interesting finding is that an increase in the deformation speed or deformation rate during drawing appears to promote conversion to the β form. The rotating speed of the drawing godets used in this work was very low (up to 18 m/min) in comparison with the drawing speeds used in industrial processes. It can be anticipated that fine tuning of the temperature during drawing will have a positive effect on β-phase formation. Another parameter not considered in this work but probably of some importance is the molecular weight of PVDF. If all these parameters are tuned in a balanced way, it seems possible to produce PVDF fibers with a high degree of crystallinity (>80%) almost completely in the β form. Such fibers would have interesting potential in intelligent textile applications in which advantage can be taken of their piezoelectric and pyroelectric properties.

CONCLUSIONS

The results of melt spinning and subsequent cold drawing have shown that cold drawing is necessary to produce fibers with β-phase crystallinity. The combined DSC and XRD analyses have shown that DSC measurements are not sufficient to provide information about the crystalline structure of PVDF. By combining a range of draw ratios in both the melt-spinning process and cold drawing, we have shown that the degree of crystallinity increases with increasing MDR and is not affected by cold drawing. This work shows that by optimization of the melt-spinning and cold-drawing parameters, PVDF fibers with a degree of crystallinity of up to 80%, mainly in the piezoelectric β form, can be prepared.

References

1. Wang, F.; Zou, Y.; Tanaka, M.; Matsuda, T.; Chonan, S. Int J Appl Electromagn Mech 2007, 25, 469.
2. Wang, F.; Tanaka, M.; Chonan, S. Int J Appl Electromagn Mech 2002, 16, 181.
3. Choi, S.; Jiang, Z. Sens Actuators A 2006, 128, 317.
4. Miyata, K.; Tanaka, M.; Nishizawa, T.; Chonan, S. Int J Appl Electromagn Mech 2006, 23, 203.
5. Mateu, L.; Moll, F., Sens Actuators A 2006, 132, 302.
6. Sajkiewicz, P.; Wasiak, A.; Goclowski, Z. Eur Polym J 1999, 35, 423.
7. Mohammadi, B.; Yousefi, A. A.; Bellah, S. M. Polym Test 2007, 26, 42.
8. Sobhani, H.; Razavi-Nouri, M.; Yousefi, A. A. J Appl Polym Sci 2007, 104, 89.
9. Sencadas, V.; Lanceros-Méndez, S.; Mano, J. F. Thermochim Acta 2004, 424, 201.
10. Lando, J. B.; Doll, W. W. J Macromol Sci Phys B 1968, 2, 205.
11. Samon, J. M.; Schultz, J. M.; Hsiao, B. S.; Seifert, S.; Stribeck, N.; Gurke, I.; Collins, G.; Saw, C. Macromolecules 1999, 32, 8121.
12. Weinhold, S.; Litt, M. H.; Lando, J. B. Macromolecules 1980, 13, 1178.
13. Bachmann, M.; Gordon, W. L.; Weinhold, S.; Lando, J. B. J Appl Phys 1980, 51, 5095.
14. Katayama, K.; Amano, T.; Nakamura, K. Kolloid-Z Z Polym 1967, 226, 125.
15. Ziabicki, A. Fundamentals of Fibre Formation; Wiley: Bath, England, 1976.
16. Cakmak, M.; Teitge, A.; Zachmann, H. G.; White, J. L. J Polym Sci Part B: Polym Phys 1993, 31, 371.
17. Wang, Y.; Cakmak, M.; White, J. L. J Appl Polym Sci 1985, 30, 2615.
18. Du, C.-H.; Zhu, B.-K.; Xu, Y.-Y. J Appl Polym Sci 2007, 104, 2254.
19. Wu, J.; Schultz, J. M.; Yeh, F.; Hsiao, B. S.; Chu, B. Macromolecules 2000, 33, 1765.
20. Wang, Y. D.; Cakmak, M. J Appl Polym Sci 1998, 68, 909.
21. Matsushige, K.; Nagata, K.; Imada, S.; Takemura, T. Polymer 1980, 21, 1391.

22. Das Gupta, D. K.; Doughty, K. Appl Phys Lett 1977, 31, 585.
23. Zhang, H.; Ren, P.; Zhang, G.-F.; Xiao, C.-F. J Wuhan Univ Technol 2006, 21, 53.
24. Li, X.; Lu, X. J Appl Polym Sci 2007, 103, 935.
25. Hasegawa, R.; Takahashi, Y.; Chatani, Y.; Tadokoro, H. Polym J 1972, 3, 600.
26. Teulings, R. P.; Dumbleton, J. H.; Miller, R. L. Polym Lett 1968, 6, 441.
27. Hattori, T.; Hikosaka, M.; Ohigashi, H. Polymer 1996, 37, 85.
28. Baltá-Calleja, F. J.; Vonk, C. G. X-Ray Scattering of Synthetic Polymers; Elsevier Science: Amsterdam, 1989.
29. Schultz, J. M.; Hsiao, B. S.; Samon, J. M. Polymer 2000, 41, 8887.
30. Samon, J. M.; Schultz, J. M.; Hsiao, B. S. Polymer 2002, 43, 1873.
31. Séguéla, R. Macromol Mater Eng 2007, 292, 235.
32. Bershtein, V. A.; Egorov, V. M. Differential Scanning Calorimetry of Polymers; Ellis Horwood: Midsomer Norton, England, 1994.
33. Van Mele, B.; Verdonck, E. Compos Interfaces 1995, 3, 83.
34. Pennings, J.; Kiel, A., Kolloid-Z Z Polym 1965, 205, 160.
35. Somani, R. H.; Yang, L.; Zhu, L.; Hsiao, B. S. Polymer 2005, 46, 8587.